The 16th Cambridge Workshop on Cool Stars, Stellar Systems and the Sun
ASP Conference Series, Vol. 448, Electronic Edition
Christopher M. Johns-Krull, Matthew K. Browning, and Andrew A. West, eds.

Starspot Imaging with the CHARA Array

J.R. Parks,[1] R.J. White,[1] G.H. Schaefer,[1,2] J.D. Monnier,[3] and G.W. Henry[4]

[1]*Department of Physics and Astronomy, Georgia State University, 29 Peachtree Center Avenue, Science Annex, Suite 400, Atlanta, GA 30303, USA; parksj@chara.gsu.edu, white@chara.gsu.edu*

[2]*Center for High Angular Resolution Astronomy, Georgia State University, Mount Wilson, CA, USA; schaefer@chara-array.edu*

[3]*Department of Astronomy, University of Michigan, 830 Dennison Bldg., 500 Church Street, Ann Arbor, MI, 48109,USA; monnier@umich.edu*

[4]*Center for Excellence in Information Systems, Tennessee State University, 3500 John Merritt Boulevard, Box 9501, Holland Hall Room 311, Nashville, TN, 37209, USA; gregory.w.henry@gmail.com*

Abstract. We present the first results of a starspot interferometric imaging program targeting the chromospherically active giant Lambda Andromedae. Our images are constructed using a new starspot model that incorporates a power limb darkening law and starspot foreshortening. The model solutions are determined through χ^2 minimization of observed squared visibilities, triple amplitudes and closure phase. Model solutions are compared with images generated from interferometric image reconstruction. We present Monte Carlo tests on the confidence of this model to recover stellar size, starspot covering factor, starspot position and temperature ratio between the starspot and surrounding photosphere. The project's results have implications on observational design and feasibility to image small scale surface structures.

1. Introduction

λ Andromedae (λ And) is a bright (M_V: 2.82 mag, M_H: 1.501 mag) G8 III classified as a RS CVn variable system due to photometric variability, chromospheric activity and high X-ray luminosity. Henry et al. (1995) performed an 11 year photoelectric survey measuring a consistent 54 day period with photometric V-band variations as large as 0.22 mag. This survey concludes photometric variability due to cool starspots on stellar surface.

Attempts have been made to map cool starspots on λ And via light curve inversion (LCI) (Donati et al. 1995; Frasca et al. 2008). LCI maps suffer from a lack of latitudinal starspot information and require an assumption of stellar inclination which is not well constrained in this case. Doppler imaging cannot be performed on this star since the v$\sin i$ = 8.5 km s^{-1}. λ And's luminosity and angular size ($\theta = 2.783 \pm 0.056$ mas) make it an ideal candidate for interferometric imaging.

2. Interferometric Imaging and Modeling

2.1. Observations and Data Reduction

Interferometric observations were taken with the Georgia State University (GSU) Center for High Angular Resolution Astronomy (CHARA) array. The CHARA array is a Y-shaped array of six 1 m telescopes providing 15 non-redundant baselines. The longest baseline (331 m) provides spatial resolutions down to ~0.5 mas.

We obtained 10 interferometric H-band observations spanning Nov. 2007 to Aug. 2008. Observations were taken using two different configurations of 4 telescopes to maximize uv sampling along particular baseline pairs. The "Outer West" configuration uses the 3 outer telescopes along with an inner telescope. The "Inner West" configuration uses the 3 inner telescopes along with an outer telescope. The observation on Nov 17^{th}, 2007 used the Inner West array. The 7 observations from Nov 17^{th}, 2008 to Sep 27^{th}, 2008 used the Outer West array. The observations on Aug 24^{th} and 25^{th}, 2009 used both configurations to achieve the greatest uv coverage.

The H-band light from the 4 telescopes was combined with the Michigan InfraRed Combiner (MIRC). We were able to collect data on 6 baselines, 4 closure phases and 4 triple amplitudes simultaneously in 8 narrow spectral channels. We employed the standard MIRC data reduction pipeline (Monnier et al. 2007). To summarize, individual frames are co-added, a mean background frame is subtracted and a Fourier transform is applied to the raw data. Squared visibilities and triple products are formed from the subsequent fringe amplitudes and phases. The flux from each telescope is calibrated via two methods, shutter matrix measurements and partial beam chopping. Final squared visibilities and triple products are obtained by calibrating system response drifts with calibrators of known size.

We also obtained differential photometry with the T3 0.40 m Automatic Photoelectric Telescope (APT) located at Fairborn Observatory. The APT is operated by the Tennessee State University (TSU) Automated Telescope Group. The APT obtained B and V band photometry on λ And from 2007 to 2010 with a 1 day cadence weather permitting. Figure 1. contains the V band and B-V color observations from the APT.

2.2. Image Reconstruction and Parametric Modeling

The data is analyzed via two independent methods: image reconstruction and parametric modeling. The image reconstructions are executed by the Markov-Chain Imager for Optical Interferometry (MACIM) (Ireland et al. 2006). We employ a limb-darkened disk (α = 0.24, (see Wittkowski et al. 2006)) as a prior in order to set the field of view and constrain flux to within the disk.

The parametrized model is a limb-darkened disk with five free parameters: stellar size, starspot size, starspot latitude, starspot longitude, and flux ratio between stellar disk and starspot. Model squared visibilities and triple products are computed via a Fourier transform of a synthetic surface generated from a given set of parameters. A solution is found through χ^2 minimization between the model data and observed data using a downhill simplex method. For a final model solution, first the stellar size is modeled by fixing starspot flux ratio of 1. The model is compared only to the first lobe of the visibility curve, which is insensitive to small scale structure (i.e. cool starspots). Next, the starspot parameters are solved for by fixing the stellar size to the modeled value. This two-step modeling procedure limits the number of free parameters and

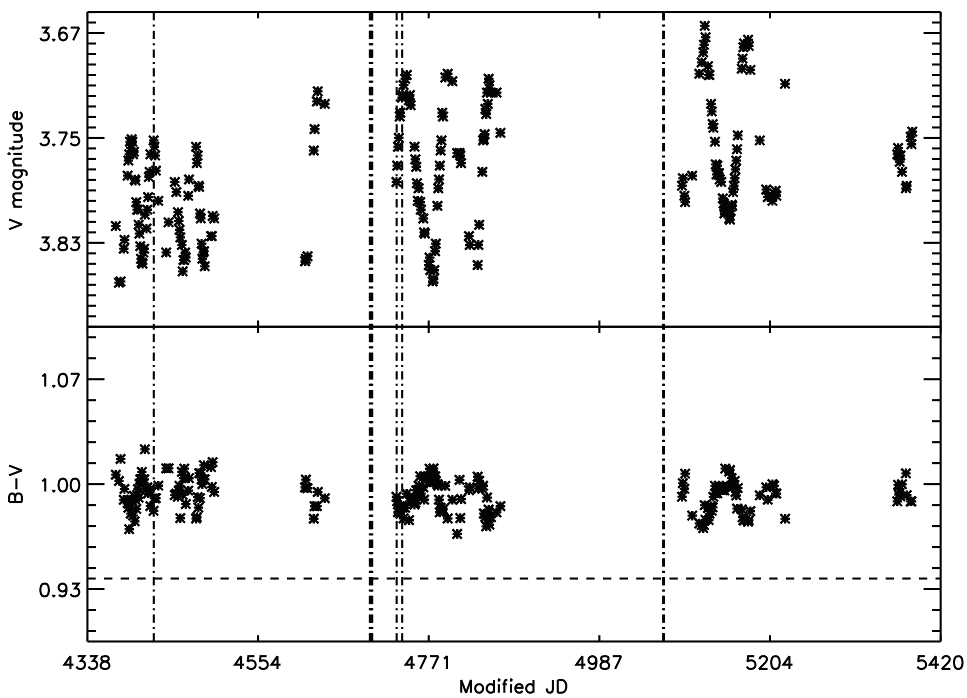

Figure 1. *Top*: V-band photometry of λ And from 2007 to 2010. Variability of 0.18 mag is likely due to cool starspots transiting stellar disk. Varying depths point to starspot evolution over the observing window. *Bottom*: B-V color curve. The horizontal dashed line represents the $(B\text{-}V)_O$ for a G8 III, λ And is red for its spectral type. The vertical lines indicate the times of interferometric observations.

helps prevent erroneous solutions due to a slightly incorrect stellar size solution. The solutions presented here are only for a single starspot model.

Figure 2. shows the present results of the MACIM image reconstructions and modeled solutions for all observations with corresponding uv sampling. The MACIM images do not provide compelling evidence for cool starspot presence and demonstrate little consistency with the modeled solutions (except for Nov. 17^{th}, 2008). This is especially notable for the observations between Nov. 17^{th} and 21^{st}, 2008. Given a rotation period of ~54 days, this observing window is too short for significant starspot motion or evolution. Within this window, the modeled solutions are more consistent with each other except for Nov 21^{st}, where the cool starspot disappears.

A potential reason for this inconsistency is limited uv sampling. For all save the last two observations, λ And was only observed twice during the night. As a result, we began observing λ And over the entire night and employing both the Outer and Inner West arrays. The observations on Aug 24^{th} and 25^{th}, 2009 used this new observing strategy. The solutions are consistent in their lack of starspots, however this is expected from the photometry on these nights (see Figure 1). These observations were taken when λ And was at the bright end of it's cycle indicating minimal or no visible starspot coverage.

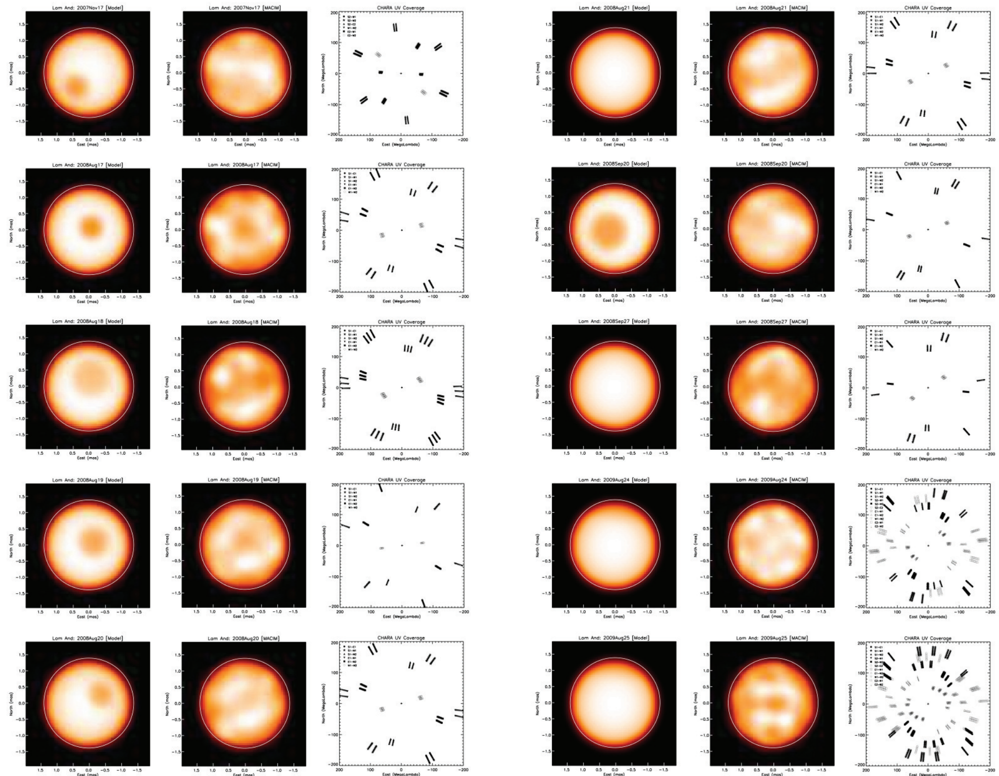

Figure 2. Faces of Lambda Andromedae. *Left Panel*: Model images. *Middle Panel*: MACIM reconstructions. *Right Panel*: UV coverage for each night. All images have been smoothed with a 0.3 mas beam. These images suffer from inconsistencies and artifacts due to poor sampling. The lack of starspot presence on Aug 24^{th} and 25^{th} 2009 is due to a lack of significant closure phases.

3. Monte Carlo Simulations

We conducted two different Monte Carlo simulations to answer the following questions: do cool starspots affect the interferometric measurement for stellar size and how does increasing the uv sampling improve model solutions. To answer these questions we generated a large number of synthetic stars with random parameters and then ran model solutions on each test star.

3.1. Stellar Size Recovery

To answer the first question, we generate 2000 synthetic stars with a random distribution of stellar size and cool starspot properties. The input parameter ranges are listed in Table 1. The range in starspot properties is consistent with those found in the literature (Berdyugina 2005). The uv sampling for each synthetic star is identical to the upper left plot in Figure 4.

Taking the Fourier transform of each synthetic star provides the "observed" visibilities. Solutions are then found by comparing modeled data to the "observed" data as described in §2.2. Again, the solutions are found by only comparing the first lobe visibility data. The results, separated into three Δ magnitude bins ranging from 0.0 to

Table 1. Monte Carlo Parameters

Parameter	Stellar Size Recovery	Starspot Properties Recovery
# of Trials	2000	500 per UV coverage
Stellar Size	1 - 5 mas	2.75 mas
LD coefficient	0.24	0.24
Covering Factor	10% - 60%	10% - 60%
Latitude	-90^o - +90^o	-90^o - +90^o
Longitude	-90^o - +90^o	-90^o - +90^o
Light Ratio	0.2 - 0.8	0.2 - 0.8
ΔMag	0.0 - 0.27 mag	0.05 - 0.25 mag

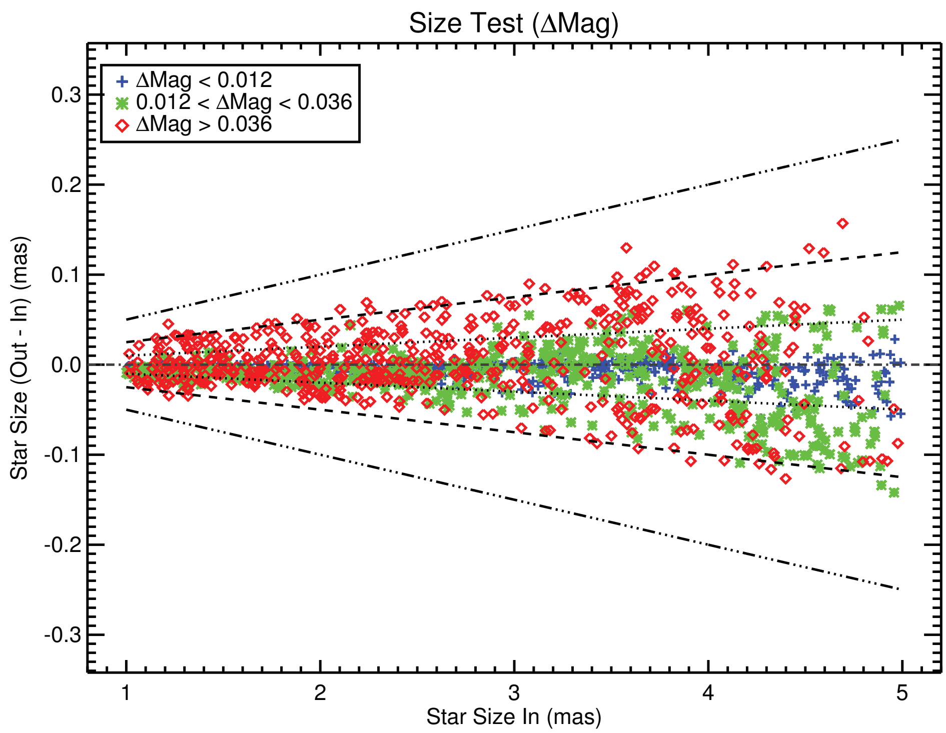

Figure 3. Results of the stellar size recovery test. The dotted line represents ~1% error. The dashed line represents ~2.5% error. The dot-dash line represents represents ~5% error. Stellar size measurements are independent of cool starspot presence to an ~2.5% precision level.

0.27 mag, are shown in Figure 4. In this case, Δ mag represents the drop in stellar magnitude due to presence of a cool starspot with respect to a unspotted star. This provides a proxy for the prominence of starspots with larger Δ magnitude indicating a larger and/or darker starspot. These results make it clear interferometric measurements of stellar diameters are insensitive to cool starspot presence to a precision of ~ 2.5%. This is evidence cool starspots are not the cause for the inflated observed M dwarf radii with respect to models (Ribas 2006).

3.2. Starspot Parameters Recovery

The second question is explored by generating 2000 synthetic stars with different levels of uv sampling. Case 1 is two mid-evening observations with the Outer West array configuration. This is very similar to the uv sampling obtained on Aug 17th, 2008. Case 2 is four observations with the Outer West array spanning the first half of the night. The Case 3 is combining Case 2 with four observations over the remainder of the night employing the Inner West configuration. The observing cadence for these three cases is 1 hour. Case 4 is identical to Case 3 except the observing cadence is now 30 minutes. Figure 4. shows the uv coverage for each trial case. Each trial case contains 500 synthetic stars.

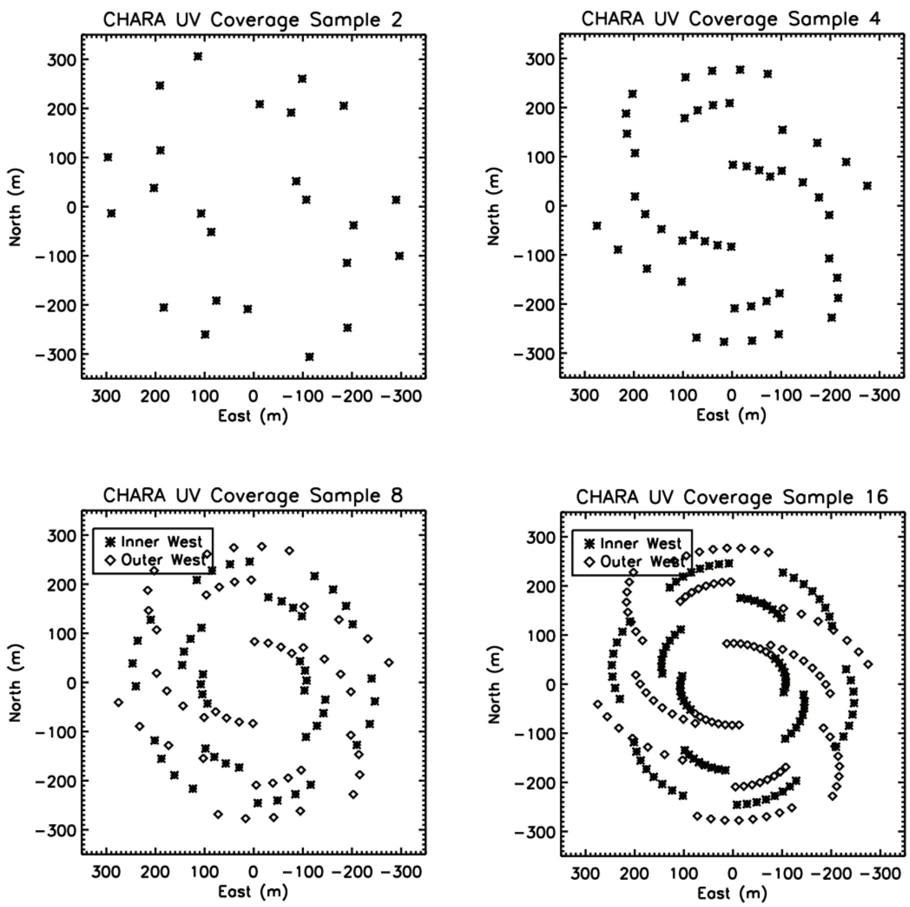

Figure 4. UV sampling used in Monte Carlo starspot recovery simulations. *Upper Left*: 2 observations with the S1, E1, W1, W2 telescopes ('Outer Array'). *Upper Right*: 4 observations with Outer Array. *Lower Left*: 4 observations with the Outer Array coupled with 4 observations with the S2-E2-W1-W2 telescopes ('Lower Array'). *Lower Right*: 8 observations with the Outer Array coupled with 8 observations with the Inner Array.

The stellar size is fixed to 2.75 mas. The starspot properties range as above, however stars are deliberated selected to fall evenly into specific Δ magnitude bins: 0.05-0.10, 0.10-0.15, 0.15-0.20, 0.20-0.25. This is investigate how starspot prominence affects recovery. Table 1. contains the input parameter ranges for this simulation. Solutions are found as described in § 2.2 where the complete visibility curve and triple products are tested. Parameters are fit simultaneously.

Solutions for this test are plotted in Figure 5. These solutions indicate no significant improvement in model fitting past 4 observations per night with the Outer West array. The large dispersion in the results maybe due to the minimization method finding local rather than global minima. The number of solutions with excellent agreement increases with improved sampling, however significant outliers inflate the dispersion resulting in the large error bars. Recovery as a function of Δ magnitude, the dispersion of solutions decreases with increased Δ magnitude. It is thus easier to precisely model a more prominent cool starspots.

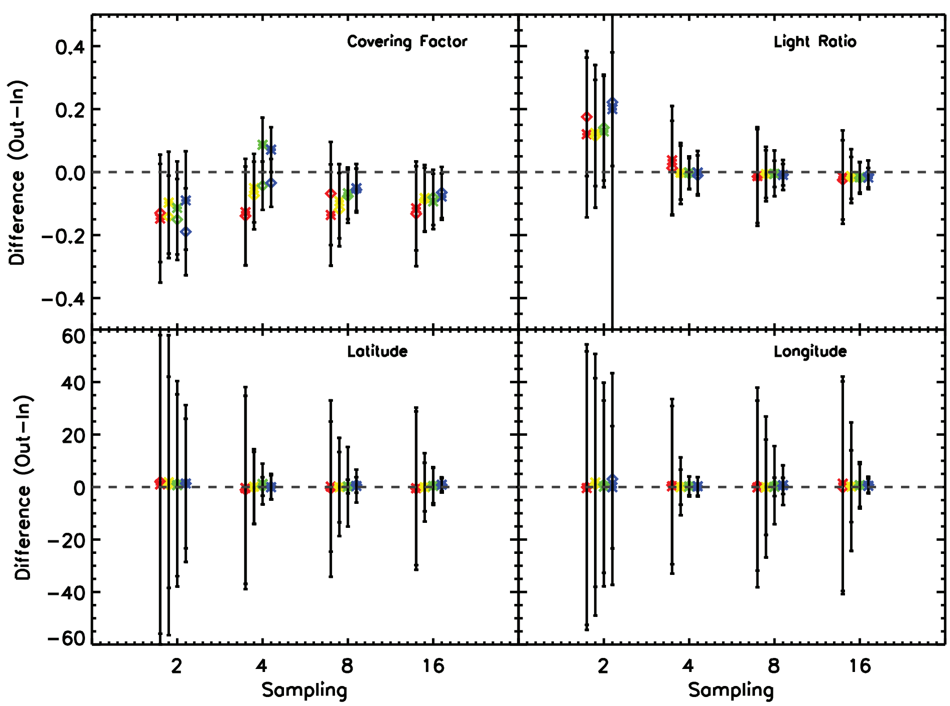

Figure 5. Starspot test results as a function of UV sampling. Data points indicate the mean difference between recovered parameters with corresponding input parameters. The error bars represent the 1σ dispersion between recovered and input parameters. *Red points*: mag bin 0.05-0.10. *Yellow points*: mag bin 0.10-0.15. *Green points*: mag bin 0.15-0.20. *Blue points*: mag bin 0.20-0.25.

Acknowledgments. We thank the CHARA Array staff and MIRC team for their considerable assistance in obtaining these observations. We would also like to thank Fabien Baron for his expertise with image reconstruction.

References

Berdyugina, S. 2005, Living Review in Solar Physics, 2, 1
Donati, J., Henry, G., & Hall, D. 1995, A&A, 293, 107
Frasca, A., Biazzo, K., Tas, G., Evren, S., & Lanzafame, A. 2008, A&A, 479, 557
Henry, G., Eaton, J., Hamer, J., & Hall, D. 1995, ApJS, 97, 513
Ireland, M., Monnier, J., & Thureau, N. 2006, in Proceedings of the SPIE (SPIE), 62681T
Monnier, J., Pedretti, E., Thureau, N., Ireland, M., Muirhead, P., Berger, J.-P., Millan-Gabet, R., Van Belle, G., ten Brummelaar, T., McAlister, H., Ridgeway, S., Turner, N., Sturmann, L., Sturmann, J., & Berger, D. 2007, Science, 317, 342
Ribas, I. 2006, in Astrophysics of Variable Stars, edited by C. Aerts & C. Sterken, vol. 349 of Astronomical Society of the Pacific Conference Series, 55
Wittkowski, M., Aufdenberg, J., Driebe, T., Roccatagliata, V., Szeifert, T., & Wolff, B. 2006, A&A, 460, 855